RESEARCH ARTICLE

Miocene age of the Huanan basalt lava flow (NE China) inferred by reset of zircon (U–Th)/He thermochronometer in the underlying sand

Jianping Zhou[1] [ID] | István Dunkl[1] | Yongjiang Liu[2,3] [ID] | Weimin Li[4] [ID] |
Anna Wolf[1] | Hilmar von Eynatten[1]

[1]Geoscience Center, Department of Sedimentology and Environmental Geology, University of Göttingen, Goldschmidtstrasse 3, Göttingen, Germany

[2]MOE Key Lab of Submarine Geoscience and Prospecting Techniques, Institute for Advanced Ocean Study, College of Marine Geosciences, Ocean University of China, Qingdao, China

[3]Laboratory for Marine Mineral Resources, Qingdao National Laboratory for Marine Science and Technology, Qingdao, China

[4]College of Earth Sciences, Jilin University, Changchun, China

Correspondence
Jianping Zhou, Geoscience Center, Department of Sedimentology and Environmental Geology, University of Göttingen, Goldschmidtstrasse 3, 37077 Göttingen, Germany.
Email: jzhou1@uni-goettingen.de

Mafic lavas of Cenozoic age are widely distributed in northeast China and received much attention as an important part of the Circum-Pacific volcanic belt. The age constraints for the volcanic activity were determined mostly by K/Ar and $^{40}Ar/^{39}Ar$ methods. We present zircon (U–Th)/He ages obtained on the thermally overprinted sands directly underlying a basaltic lava. This thermochronometer is insensitive to weathering and not biased by excess argon, thus it can express accurately the age of thermal effect of the lava flow. As a regional cooling age reference, three granite samples were dated from basement units that have not been thermally influenced by the basalt eruptions. The reference granite samples revealed well-defined Cretaceous (U–Th)/He-ages, while 20 zircon crystals from the sand below the basalt lava revealed a prominent Miocene (U–Th)/He age component of 9.33 ± 0.24 Ma. Raman spectroscopy of these zircon crystals supports their thermally overprinted character. We infer that the sand sample has experienced significant thermal overprint by the overlying basalt lava leading to thermal reset of the majority of the detrital zircon crystals. The obtained age is thus interpreted as the eruption age of the basalt lava. The Huanan basalt flow thus belongs to volcanics of the Laoyeling episode in NE China.

KEYWORDS
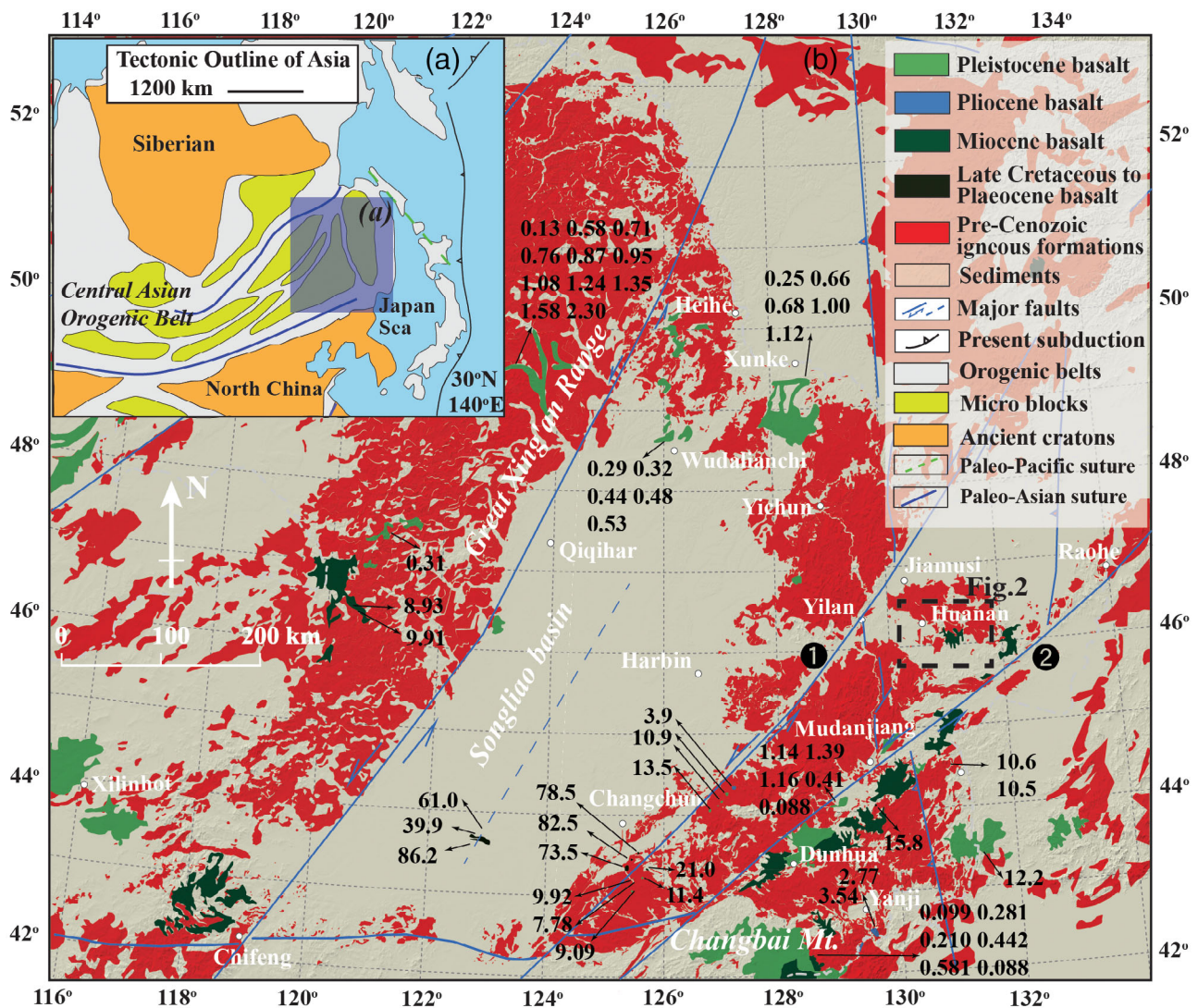(U–Th)/He, basaltic lava, Huanan, Miocene, NE China, Raman

FIGURE 1 (a) Simplified geological map of NE China, modified after Ren et al. (2013) and HBGMR (1993). The occurrences of basalt volcanoes and their age (in Ma) are taken from Fan, Sun, Li, and Wang (2006), Fan et al. (2011), Fan, Zhao, Sui, Li, and Wu (2012), Liu (1987), Liu, Chen, Zhong, Lin, and Wang (2017), Liu et al. (2017), Qiu, Liao, and Liu (1991), and Zhang, Xu, Ge, and Ma (2006). The digital elevation model is from the U.S. Geological Survey, 2017. The two faults marked with (1) and (2) are the Jiamusi–Yitong and Dunhua–Mishan faults, respectively, and belong to the eastward extension of the Tan–Lu Fault Zone in NE China. Dashed box indicates position of Figure 2. (b) Schematic tectonic map of North Asia (modified after Liu, Chen, et al., 2017; Liu, Li, et al., 2017) [Colour figure can be viewed at wileyonlinelibrary.com]

1 | INTRODUCTION

Mafic lavas of Cenozoic age are widely distributed in northeast China. Despite the small size of these occurrences, they represent an important part of the Circum-Pacific volcanic belt (Basu, Wang, Huang, Xie, & Mitsunobu, 1991; Flower, Tamaki, & Hoang, 1998; Zou, Fan, & Yao, 2008; Xu et al., 2015). The age constraints of this volcanic activity were determined mostly by K/Ar and ^{40}Ar/^{39}Ar methods and range from Miocene to Pleistocene except for some Late Cretaceous to Paleogene ages within and east of the Songliao Basin (Figure 1; Fan, Sui, Wang, Li, & Sun, 2007; Hu et al., 1983; Liu, 1987; Liu, Chen, et al., 2017; Liu, Li, et al., 2017; Qiu et al., 2007; Wang et al., 1983; Zheng, Xu, & Wang, 1999; Zhang et al., 2006).

In the last two decades, new geochronological techniques were introduced for dating young mafic eruptions such as the U–Th disequilibrium method (Zou, Zindler, Xu, & Qi, 2000), indirect dating of volcanics from the surrounding fallout organic material deposits by the ^{14}C method (Xu, Zhang, Qiu, Ge, & Wu, 2012; Yin et al., 2012), fission track dating of volcanic glasses (Renne, 2000), and magnetite or zircon (U–Th)/He (ZHe) geo-thermochronology (e.g., Blackburn, Stockli, & Walker, 2007; Blondes, Reiners, Edwards, & Biscontini, 2007; Cooper, van Soest, & Hodges, 2011; Farley, 2002). The modern ^{40}Ar/^{39}Ar approaches may yield precise ages of young volcanic rocks, but typically the age of young and/or low-K lava samples have high errors due to minor proportions of radiogenic Ar (Blondes et al., 2007; McDougall & Harrison, 1999). The magnetite (U–Th)/He method is

also introduced to date mafic volcanic rocks (Blackburn et al., 2007; Fanale & Kulp, 1962). However, this mineral is not suitable for a wide range of applications due to its disadvantages. For example, (a) the Fe-oxide minerals in mafic volcanic formations have frequently irregular external morphology, thus the ejection (FT) correction is hardly feasible and it would generate significant bias (Hernandez Goldstein, Stockli, Ketcham, & Seman, 2014). (b) The interior of the magnetite grains in lavas are highly heterogeneous, often penetrated by ilmenite and haematite lamellae and they contain apatite inclusions. (c) The U content is usually very low. The studies for example, Fanale and Kulp (1962) and Blackburn et al. (2007) were dealing with pre-Cenozoic ages, with a few ppm or even sub-ppm uranium content. In the case of Miocene–Pliocene lavas the uncertainties would be much over the expectations for stratigraphical purposes. Furthermore, the Blackburn et al. (2007) study was made on kimberlites, which has atypical actinide contents and distributions.

Zircon analysis has been proven a versatile tool for examining a wide range of geological processes because zircon crystals have a lot of important features for geochronology and thermochronology including high actinide concentrations, occurrence in variable lithologies and resistance to physical and chemical weathering (Reiners, 2005). Like many other minerals, zircon can also be dated by the (U–Th)/He method to reveal the low temperature (~180–130°C) thermal history (e.g., Farley, 2002; Reiners, Spell, Nicolescu, & Zanetti, 2004). Comparing to the K/Ar and $^{40}Ar/^{39}Ar$ methods, zircon (U–Th)/He method has the advantage of performing relatively rapidly on selected zircon crystals without neutron irradiation, and high accuracy on young volcanic rocks (Blondes et al., 2007). Even though mafic to intermediate volcanic rocks rarely contain zircon crystals, the strata below lava flows or the host rocks in contact with basaltic dykes, sills, or necks are often rich in zircon crystals. These zircons may become thermally reset upon significant heating (temperature and time) and the (U–Th)/He age obtained on these crystals then indicates cooling after the heating event. Assuming usual fast cooling of lava flows, this age should reflect the eruption age (Blondes et al., 2007; Cooper et al., 2011).

In this study, we report for first time zircon (U–Th)/He ages from a thermally overprinted basal layer of a lava flow from the Huanan region in NE China. Additionally, Raman spectroscopy was used to describe the crystalline state and confirm the thermal reset of the dated zircon crystals.

2 | GEOLOGICAL SETTING

NE China is enclosed by the Siberian Block in the north, the North China Block in the south and the Pacific Plate in the east, tectonically situating in the eastern segment of the world's largest accretionary orogen, the Central Asian Orogenic Belt (CAOB; Jahn et al., 2000; Sengör et al., 1993; Windley et al., 2007; Figure 1). This area was mainly dominated by the Palaeo-Asian Ocean tectonic domain in the Pre-Mesozoic period, and strongly transformed by the circum-Pacific

tectonic domain since the Mesozoic (Liu et al., 2010, 2017). Since the Late Mesozoic a large continental rift system developed in NE China, related to the subduction of the Pacific Plate and back-arc extension of the Japan Sea (Liu, 1988; Xu & Fan, 2015). This rift system includes the Songliao Basin, Jiamusi–Yitong Fault Zone, Dunhua–Mishan Fault Zone, and other adjacent basins (Figure 1). Contemporaneously, about 690 volcanic cones and craters and 50,000 km² of basaltic lavas with small amounts of alkali trachyte were formed in this area. The Cenozoic volcanism is mainly distributed alongside a series of NE to NNE-oriented rift basins and adjacent mountain ranges and on both sides of the Songliao Basin, but major volcanic activity occurred to the east (Liu, 1988; Figure 1). From west to east, the distribution of the volcanic rocks can be divided into several zones, these are the Great Xing'an Range, the Jiamusi–Yitong Fault Zone, the Dunhua–Mishan Fault Zone and the Changbai Mountains. The borehole data from the Songliao Basin reveals over 1 km-thick Palaeogene basalt bodies of tholeiitic composition (Xu et al., 2015). The next volcanic activity peak period appeared in the Neogene and mainly follows the Jiamusi–Yitong Fault Zone and Dunhua–Mishan Fault Zone. The youngest Quaternary volcanic rocks in NE China are distributed around the Songliao Basin with major occurrences in the Great Xing'an Range and even more western areas, to the north of the Songliao Basin, and to the east in the Changbai Mountains, mostly east of Dunhua–Mishan Fault Zone (Bai, Tian, Wu, Xu, & Li, 2005; Bai, Wang, Xu, Liu, & Xu, 2008; Fan & Hooper, 1991; Fan, Liu, Zhang, & Sui, 1998; Fan et al., 1999, 2006, 2007, 2011, 2012; Liu, 1987; Liu et al., 1998; Qiu et al., 1991; Zhang et al., 2000; Zhao et al., 2008; Figure 1). The Cenozoic basalts in NE China are considered products of partial melting of the upper mantle, and mixing of depleted mantle and enriched mantle Type I components (Xu et al., 2015; Zou et al., 2000, Zhou, 2006).

Even though numerous geochronological studies have been published from many occurrences of mafic volcanic formations in NE China, high-precision and weathering-insensitive geochronology such as zircon U–Pb or (U–Th)/He dating has not yet been performed on the young volcanic formations of the Huanan area. Previous studies in this area mainly rely on constraints from lithostratigraphic and paleontological evidences (HBGMR, 1993).

3 | SAMPLE AND ANALYTICAL METHODS

A sand sample (JB40) was collected in an active basalt quarry close to Qunli village (Figure 2; 46.2983°N, 130.7182°E). A 2–3 m thick horizontal lava flow is exposed along the excavation walls and the contact to the underlying sand is well preserved and accessible. In the surroundings of the quarry, the sand forms only a few metres thick layer; this young, alluvial sediment covers the granitoid basement. The basal layer of the lava is amygdaloid, but the lava shows a low degree of alteration. We collected a loose sand sample from the topmost 3–5 cm, immediately below the base of the basalt lava (Figure 3).
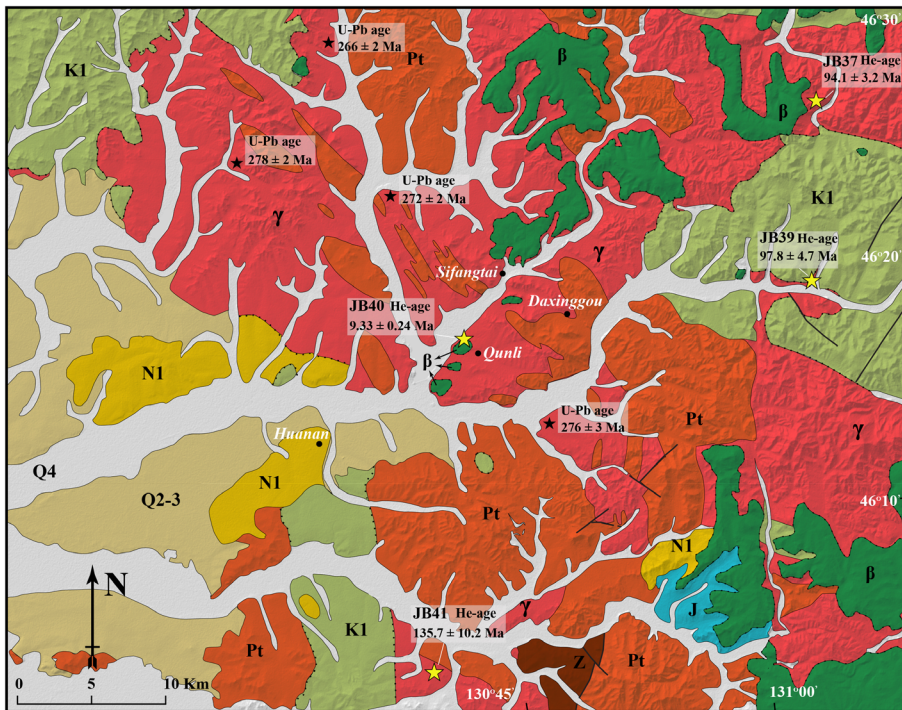
FIGURE 2 Simplified geological map of the study area, modified after HBGMR (1993). The digital elevation model is taken from the U.S. Geological Survey, 2017. Pt, Palaeoproterozoic strata; J, Jurassic strata; K1, lower Cretaceous strata; N1, Miocene strata; Q2-3, Middle to Upper Quaternary strata; Q4, Holocene strata; γ: Permian granite; β: Cenozoic basalt; yellow star: sample locations in this article and the measured (U–Th)/He age; black star: zircon U–Pb age of granitoids (Dong et al., 2017); Solid black lines: faults; dotted black lines: unconformities [Colour figure can be viewed at wileyonlinelibrary.com]

FIGURE 3 Photographs illustrating the basalt lava outcrop and its base close to Qunli village. Thickness of the lava flow in the upper left photo is 2–3 m with sand below [Colour figure can be viewed at wileyonlinelibrary.com]

To discriminate the thermal influence imposed by the basalt lava to the underlying granite basement at the sampling position and the untouched area, three granite samples were collected for (U–Th)/He dating from the wider area surrounding the basalt quarry (Figure 2; JB37, 46.4320°N, 131.09425°E; JB39, 46.3189°N, 131.0713°E; JB41, 46.0767°N; 130.6672°E). The zircon grains were separated from the 63–125 μm fraction by shaking table, gravity separation by Na-poly-tungstate, and magnetic separation.

The zircon crystals have variable shapes and colours, but they are mostly pinkish-brown, transparent-translucent and euhedral to slightly rounded. (U–Th)/He analyses were performed at the GÖochron Laboratory of the Geoscience Center, University of Göttingen. Twenty-eight intact zircon crystals were selected by stereo- and petrographic microscopes. The crystals were photographed and their dimensions (length, width, and prismatic length) were used for alpha-ejection correction (Farley, Wolf, & Silver, 1996; Figure 4). The grains were wrapped in
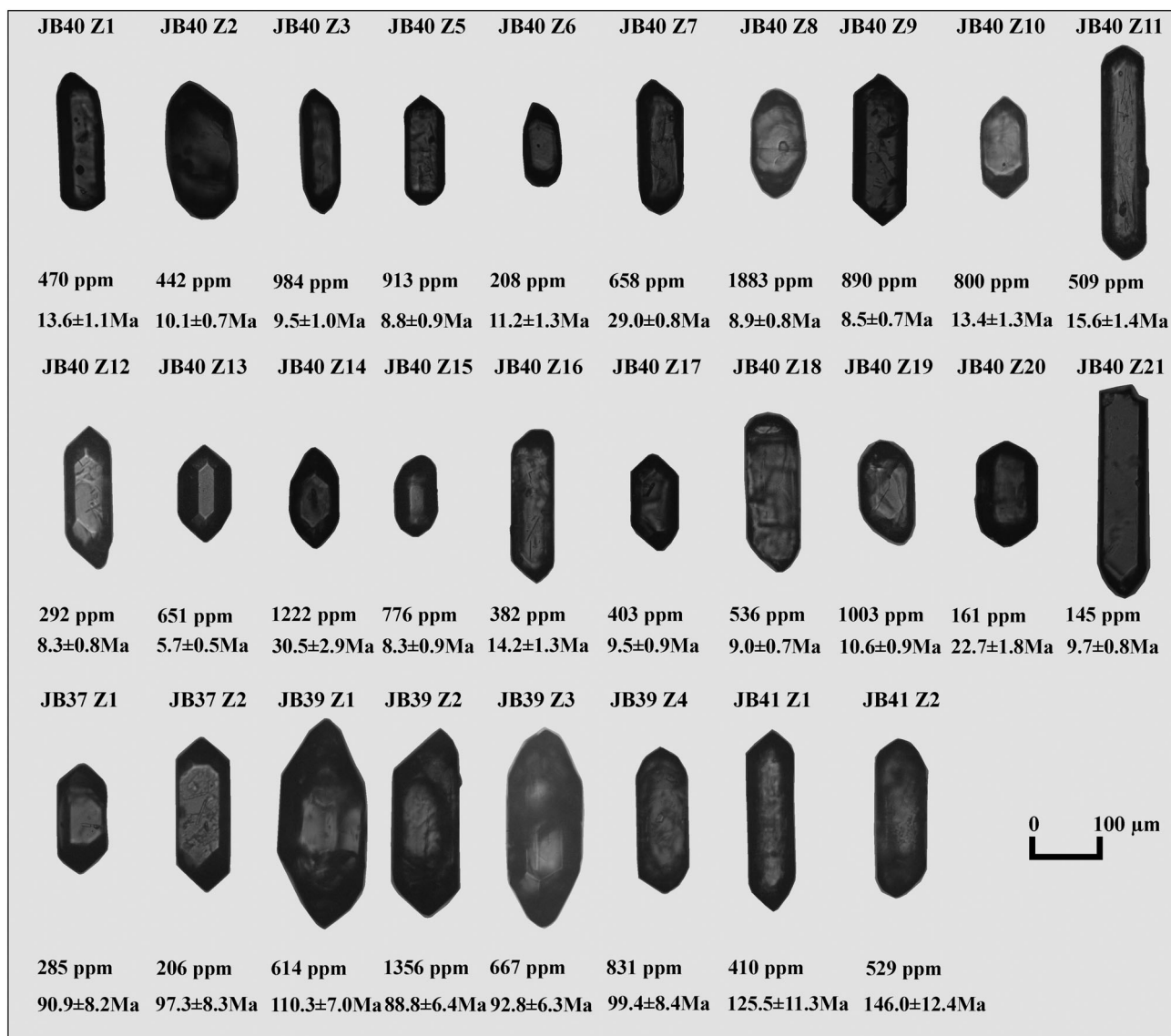
FIGURE 4 Microphotographs of the dated zircon crystals along with the effective U concentration (eU, where eU is calculated as U + 0.235 * Th; Gordon Gastil, DeLisle, & Morgan, 1967) and the (U–Th)/He age

platinum capsules for helium extraction and heated with an infrared laser. The extracted gas was purified by an SAES Ti-Zr getter at 450°C. The remaining inert gas was measured by a Hidden triple-filter quadrupole mass spectrometer equipped with a positive ion-counting detector.

Following degassing, the capsules were retrieved from the gas extraction line the zircon crystals were extracted from the capsules and spiked with calibrated ^{230}Th and ^{233}U solutions in 0.4 ml teflon vials. The crystals were dissolved for 5 days at 220°C in pressurized bombs using a mixture of double distilled 48% HF and 65% HNO$_3$. Each sample batch was prepared with a series of procedural blanks and spiked normals to check the purity and calibration of the reagents and spikes. Spiked solutions were analysed by a Thermo iCAP Q ICP-MS. Procedural U and Th blanks by this method are usually very stable in a measurement session and below 1.5 pg. The ejection correction factors (Ft) were determined for the single crystals by a modified algorithm of Farley et al. (1996) using an in-house spread sheet.

Raman spectroscopy was applied to all zircon samples to identify the thermal influence on the lattice of the zircon crystals as additional information to interpret the (U–Th)/He chronological data. Details of the laboratory procedure can be found in Lünsdorf and Lünsdorf (2016). The IFORS software was used to evaluate the Raman spectra. Fitted peak widths were corrected for the apparatus function after Irmer (1985) and Nasdala et al. (2001).

4 | RESULTS

4.1 | Zircon (U–Th)/He ages

Twenty-eight euhedral or slightly rounded zircon crystals were dated (Figure 4 and Table 1). The crystal sizes with c-axis parallel and perpendicular dimensions range from 120 to 319 μm and 55 to 98 μm,

TABLE 1 Zircon (U-Th)/He results obtained on the sand and granite samples in this study

Sample	He Vol. [ncc]	He 1s [%]	238U- Mass [ng]	1s [%]	Conc. [ppm]	232Th- Mass [ng]	1s [%]	Conc. [ppm]	Th/U ratio	Sm Mass [ng]	1s [%]	Conc. [ppm]	eU [ppm]	Sphere radius [μm]	Ejection correct. (Ft)	Uncorr. He-age [Ma]	Ft-Corr. He-age [Ma]	2s [Ma]	Sample unweigted aver. ± 1 SE He-age [Ma]	2s [Ma]
JB40 z1	1.436	1.1	1.081	1.8	447.7	0.232	2.4	96	0.21	0.016	3.1	7	470.3	53	0.769	10.5	13.6	1.1		
JB40 z2	1.756	1.1	1.713	1.8	417.8	0.425	2.4	104	0.25	0.012	3.1	3	442.1	59	0.791	8.0	10.1	0.7		
JB40 z3	1.418	1.1	1.752	1.8	937.1	0.371	2.4	199	0.21	0.019	3.1	10	983.7	36	0.672	6.4	9.5	1.0		
JB40 z5	0.734	1.1	0.922	1.8	831.4	0.387	2.4	349	0.42	0.012	3.1	11	913.4	37	0.679	6.0	8.8	0.9		
JB40 z6	0.179	1.6	0.181	2.2	186.2	0.092	2.5	95	0.51	0.007	3.1	8	208.4	34	0.652	7.3	11.2	1.3		
JB40 z7	5.636	1.0	2.107	1.8	614	0.641	2.4	187	0.30	0.015	5.5	4	658.3	42	0.711	20.6	29.0	2.8		
JB40 z8	2.100	1.1	2.627	1.8	1861	0.136	2.4	96	0.05	0.005	5.5	4	1883.3	46	0.735	6.5	8.9	0.8		
JB40 z9	3.226	1.0	3.896	1.8	836	1.051	2.4	226	0.27	0.022	5.5	5	889.5	51	0.758	6.4	8.5	0.7		
JB40 z10	2.605	1.0	2.176	1.8	762	0.456	2.4	160	0.21	0.008	5.5	3	799.5	41	0.706	9.4	13.4	1.3		
JB40 z11	2.736	1.1	1.897	1.8	480	0.488	2.4	123	0.26	0.023	5.5	6	508.8	44	0.723	11.3	15.6	1.4		
JB40 z12	0.831	1.2	1.081	1.8	277	0.248	2.4	64	0.23	0.017	5.5	4	291.7	44	0.727	6.0	8.3	0.8		
JB40 z13	0.765	1.2	1.441	1.8	618	0.325	2.4	140	0.23	0.056	5.5	24	650.9	45	0.734	4.2	5.7	0.5		
JB40 z14	9.985	1.0	3.738	1.8	1,200	0.298	2.4	96	0.08	0.007	5.5	2	1,222.4	41	0.711	21.7	30.5	2.9		
JB40 z15	0.719	1.2	1.032	1.8	750	0.156	2.4	114	0.15	0.005	5.5	3	776.4	36	0.671	5.6	8.3	0.9		
JB40 z16	1.539	1.1	1.185	1.8	361	0.290	2.4	88	0.25	0.017	5.5	5	382.0	42	0.714	10.2	14.2	1.3		
JB40 z17	0.775	1.2	0.901	1.8	380	0.238	2.4	100	0.26	0.011	5.5	4	403.4	41	0.707	6.7	9.5	0.9		
JB40 z18	2.153	1.0	2.447	1.8	505	0.653	2.4	135	0.27	0.042	5.5	9	536.4	52	0.764	6.9	9.0	0.7		

TABLE 1 (Continued)

| Sample	He Vol. [ncc]	He 1s [%]	^{238}U Mass [ng]	^{238}U 1s [%]	^{238}U Conc. [ppm]	^{232}Th Mass [ng]	^{232}Th 1s [%]	^{232}Th Conc. [ppm]	Th/U ratio	Sm Mass [ng]	Sm 1s [%]	Sm Conc. [ppm]	eU [ppm]	Sphere radius [µm]	Ejection correct. (Ft)	Uncorr. He-age [Ma]	Ft-Corr. He-age [Ma]	Ft-Corr. 2s [Ma]	Sample unweighted aver. ± 1 SE He-age [Ma]	Sample unweighted aver. ± 1 SE 2s [Ma]
JB40 z19	3.319	1.1	3.335	1.8	958	0.660	2.4	190	0.20	0.010	5.5	3	1,003.0	48	0.745	7.9	10.6	0.9	10.6	
JB40 z20	1.227	1.1	0.529	1.8	146	0.236	2.4	65	0.45	0.021	5.5	6	160.9	52	0.763	17.3	22.7	1.8		
JB40 z21	0.633	1.3	0.650	1.8	129	0.338	2.4	67	0.52	0.032	5.5	6	144.6	47	0.741	7.2	9.7	0.8		
JB37 z1	7.550	1.2	0.857	1.8	261	0.329	2.4	100	0.38	0.017	6.5	5	284.7	45	0.732	66.5	90.9	8.2		
JB37 z2	11.127	1.2	1.178	1.8	194	0.317	2.4	52	0.27	0.025	6.5	4	205.9	49	0.751	73.1	97.3	8.3	94.1	3.2
JB39 z1	88.920	1.2	7.681	1.8	597	0.931	2.4	72	0.12	0.070	6.5	5	614.1	77	0.838	92.5	110.3	7.0		
JB39 z2	99.685	1.2	11.233	1.8	1,331	0.919	2.4	109	0.08	0.084	6.5	10	1,356.3	64	0.807	71.7	88.8	6.4		
JB39 z3	61.323	1.2	6.356	1.8	638	1.252	2.4	126	0.20	0.052	6.5	5	667.2	68	0.818	75.9	92.8	6.3		
JB39 z4	26.639	1.2	2.790	1.8	793	0.563	2.4	160	0.20	0.034	6.5	10	830.7	50	0.755	75.0	99.4	8.4	97.8	4.7
JB41 z1	20.940	1.2	1.756	1.8	385	0.495	2.4	109	0.28	0.099	6.5	22	410.4	45	0.732	91.9	125.5	11.3		
JB41 z2	33.814	1.2	2.419	1.8	507	0.450	2.4	94	0.19	0.070	6.5	15	529.3	49	0.753	109.9	146.0	12.4	135.7	10.2
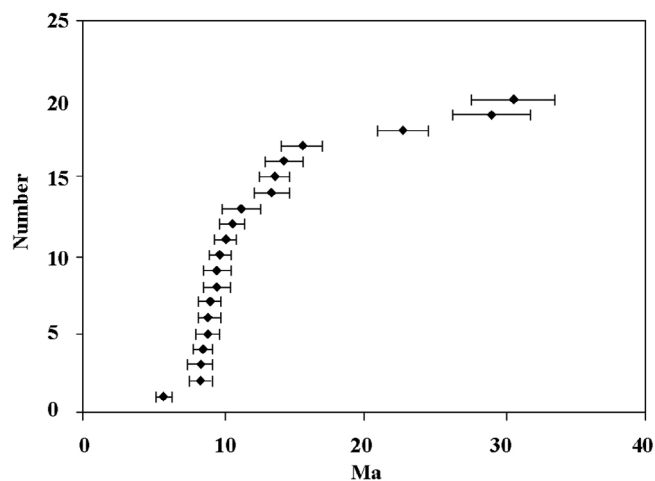
FIGURE 5 Cumulative diagram of zircon (U–Th)/He ages obtained on 20 single crystals from the sand sample (JB40; 2σ error bars)
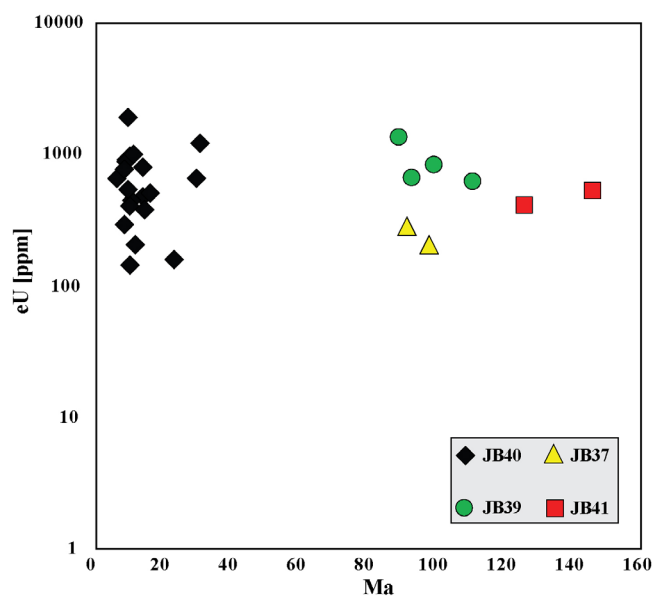

FIGURE 6 Effective U concentration (eU) versus zircon (U–Th)/ He ages plot for the sand sample JB40 and the three granitoid samples. Each symbol represents a single dated zircon crystal [Colour figure can be viewed at wileyonlinelibrary.com]

respectively. The measured zircon crystals reveal radii ranging from 34 to 59 μm and the effective uranium concentration (eU, where eU is calculated as [U ppm] + 0.235 * [Th ppm]; Gordon Gastil et al., 1967) covers a wide range from 145 to 1883 ppm. The Ft-corrected zircon ZHe ages of the dated crystals from the JB40 sand sample range from 5.7 to 30.5 Ma (Figures 4 and 5). Except for the youngest single zircon He age of 5.7 ± 0.5 Ma and three older He-ages >20 Ma, the ages reveal a tight distribution between 8.3 and 15.6 Ma. The Ft-corrected ZHe ages of the three granite samples from the region also reveal tight clustering with unweighted ZHe mean ages of 94.1 ± 3.2, 97.8 ± 4.7, and 135.7 ± 10.2 Ma for samples JB37, JB39, and JB41, respectively (Table 1). ZHe ages show no correlation with eU concentrations (Figure 6) implying that the effect of radiation damage density on the

measured apparent (U–Th)/He ages is negligible (e.g., Cook, Royden, Burchfiel, Lee, & Tan, 2013; Flowers, Ketcham, Shuster, & Farley, 2009; Reiners, 2005; Shuster, Flowers, & Farley, 2006).

4.2 | Raman spectra of the zircon crystals

ZHe ages are determined by the retentivity of He in zircon crystals, which is influenced by the alpha-damage inflicted in its crystalline lattice due to self-irradiation (e.g., Guenthner, Reiners, Ketcham, Nasdala, & Giester, 2013). Raman spectroscopy offers the opportunity to quantify the degree of metamictization in zircon crystals (Nasdala, Irmer, & Wolf, 1995) selected for (U–Th)/He analysis. The accumulated alpha-damage is estimated from the position and the width of the $\nu_3(SiO_4)$ Raman band, the stretching vibration of the SiO_4 tetrahedra about 1,000 cm^{-1} (Dawson, Hargreave, & Wilkinson, 1971). In our case, the four samples reveal distinct, narrow internal, and external vibrational modes in the spectral range from 972.1 to 1,010.5 cm^{-1}. All of the analysed zircon crystals have tightly distributed full width at half-maximum (FWHM) values ranging from 3.4 to 9.0 cm^{-1}, with averages of 5.1 cm^{-1} (JB40), 5.5 cm^{-1} (JB37), 5.2 cm^{-1} (JB39), and 6.8 cm^{-1} (JB41), respectively (Table 2).

5 | DISCUSSION

5.1 | Identification of the principal age component of the single-crystal ZHe data

Visualizing and interpreting the ages obtained on detrital zircon crystals forms a key part to unravel the corresponding geological questions in detrital zircon geochronological and thermochronological studies. The probability density plot (PDP) and the kernel density estimate (KDE) are the most used methods for visualizing detrital age distributions (Devroye, 1987; Hurford, Fitch, & Clarke, 1984; Silverman, 1986; Vermeesch, 2012; von Eynatten & Dunkl, 2012). However, it has been pointed out that the PDP lacks any theoretical basis as a probability density estimator, although it may serve as a data visualization tool (Galbraith, 1998, 2010; Vermeesch, 2012).

The ZHe age distribution is visualized as KDE plot by the DensityPlotter v8.4 software (Figure 7; Vermeesch, 2012). The KDE age spectrum shows a typical left-hand asymmetry and the mean of the dominating (about 75%) youngest age component is 9.33 ± 0.24 Ma (Figure 7). To further corroborate the result, we also use the SIMPLEX method (Cserepes, 1989) to perform a best-fit model to identify the age components by the Popshare software (Dunkl & Székely, 2002). This approach results in a similar best-fit model age at 9.2 ± 0.8 Ma.

5.2 | Zircon reset analysis

In the study area, most of the basalt lava overlies the basement dominated by granitoid rocks. In our study site, the lava covers alluvial

TABLE 2 The $v_3(SiO_4)$ Raman band of the zircon samples investigated

Sample	Aliquot	Scale intensity	Shape	Area	HWHM [cm⁻¹]	Centre [cm⁻¹]	Scaled_intensity	Shape	Area	HWHM [cm⁻¹]	Corr FWHM [cm⁻¹]	Centre [cm⁻¹]
JB40	JB_Points00	13.426	0.930	636.008	3.076	976.246	91.795	0.780	4,179.228	3.102	4.9	1,009.286
	JB_Points01	12.933	0.984	674.038	3.334	976.246	84.662	0.775	4,141.691	3.342	5.5	1,009.482
	JB_Points02	12.898	0.979	738.396	3.676	976.246	90.315	0.842	4,543.066	3.363	5.5	1,009.286
	JB_Points03	12.050	0.687	459.716	2.677	977.028	85.441	0.516	3,145.437	2.744	3.9	1,010.459
	JB_Points04	8.149	0.987	312.851	2.439	977.419	45.620	0.513	1,615.646	2.641	3.6	1,010.459
	JB_Points05	14.672	0.983	626.901	2.723	976.833	90.120	0.769	4,189.730	3.180	5.1	1,010.264
	JB_Points12	11.592	0.986	608.307	3.356	975.660	76.930	0.820	3,961.219	3.468	5.8	1,008.895
	JB_Points13	13.924	0.988	789.011	3.629	975.269	89.816	0.857	4,969.772	3.687	6.3	1,008.113
	JB_Points14	10.022	0.916	641.540	4.207	975.464	67.544	0.988	4,322.868	4.105	7.3	1,008.309
	JB_Points15	14.272	0.866	558.459	2.586	976.246	91.525	0.643	3,845.737	2.997	4.6	1,009.482
	JB_Points16	7.732	0.982	364.740	3.013	976.051	48.804	0.358	1900.080	3.082	4.8	1,009.873
	JB_Points17	13.463	0.717	526.283	2.716	976.051	93.207	0.671	3,828.205	2.899	4.4	1,009.286
JB41	JB_Points21	13.021	0.861	563.778	2.871	975.269	92.677	0.792	4,212.499	3.084	4.8	1,008.700
	JB_Points22	13.290	0.683	554.084	2.934	975.073	94.072	0.740	4,279.829	3.141	5.0	1,008.504
	JB_Points23	13.562	0.821	610.673	3.028	975.269	93.998	0.794	4,529.139	3.270	5.3	1,008.309
	JB_Points24	8.590	0.985	341.875	2.532	975.269	46.711	0.489	1933.924	3.121	4.9	1,008.504
	JB_Points25	6.530	0.616	319.489	3.535	974.682	41.671	0.467	1,753.101	3.198	5.1	1,008.113
	JB_Points27	13.464	0.811	645.952	3.241	974.878	90.224	0.876	4,971.491	3.650	6.2	1,008.113
	JB_Points28	13.114	0.832	553.772	2.826	974.878	88.163	0.738	4,033.348	3.161	5.0	1,007.722
	JB_Points29	13.946	0.882	625.333	2.956	974.878	92.535	0.883	4,777.977	3.408	5.6	1,008.113
	JB_Points30	4.954	0.986	380.491	4.968	972.727	39.097	0.990	2,682.392	4.406	7.9	1,004.399
	JB_Points31	13.613	0.969	794.396	3.763	972.923	86.804	0.935	5,506.929	4.137	7.3	1,005.767
	JB_Points33	48.511	0.887	2,227.010	3.021	974.878	75.363	0.793	3,693.487	3.328	5.5	1,007.918
	JB_Points35	46.715	0.694	1,861.382	2.792	974.682	61.053	0.964	3,015.706	3.172	5.1	1,007.722
	JB_Points36	13.907	0.601	542.355	2.822	975.464	93.989	0.635	3,837.965	2.920	4.4	1,008.504
	JB_Points37	14.625	0.846	679.106	3.099	975.073	93.083	0.825	4,548.809	3.283	5.3	1,008.309
	JB_Points38	15.011	0.743	641.999	2.949	975.269	92.643	0.761	4,196.505	3.105	4.9	1,008.309
JB37	JB_Points45	13.185	0.976	772.149	3.768	974.682	92.345	0.851	5,503.284	3.986	7.0	1,007.918
	JB_Points46	12.667	0.920	808.400	4.190	973.900	90.245	0.812	6,147.744	4.631	8.4	1,006.549
	JB_Points47	13.016	0.982	865.969	4.288	973.705	93.783	0.817	6,372.261	4.612	8.4	1,006.354
	JB_Points49	13.936	0.890	646.904	3.053	975.073	95.068	0.788	4,783.881	3.425	5.7	1,008.113
	JB_Points50	13.289	0.900	610.030	3.009	974.291	92.751	0.760	4,488.373	3.322	5.4	1,007.136
	JB_Points51	13.720	0.885	604.090	2.898	975.660	92.609	0.751	4,302.652	3.197	5.1	1,008.895

(Continues)

TABLE 2 (Continued)

Sample	Aliquot	Scale intensity	Shape	Area	HWHM [cm⁻¹]	Centre [cm⁻¹]	Scaled_intensity	Shape	Area	HWHM [cm⁻¹]	Corr FWHM [cm⁻¹]	Centre [cm⁻¹]
	JB_Points52	13.332	0.653	526.979	2.809	975.269	94.097	0.676	4,112.200	3.083	4.8	1,008.700
	JB_Points53	13.421	0.681	532.055	2.790	975.464	92.573	0.688	4,023.187	3.053	4.8	1,008.895
	JB_Points54	12.294	0.627	480.804	2.804	975.660	92.312	0.663	3,591.145	2.752	4.0	1,008.504
	JB_Points55	13.523	0.700	552.100	2.855	975.269	90.668	0.731	4,065.666	3.105	4.9	1,008.504
	JB_Points56	13.462	0.783	555.673	2.807	975.464	92.266	0.724	3,984.224	2.995	4.6	1,008.504
	JB_Points57	13.177	0.860	640.517	3.232	975.073	96.727	0.798	4,915.740	3.448	5.7	1,008.113
	JB_Points58	13.353	0.796	558.328	2.831	975.464	92.076	0.726	4,141.994	3.120	4.9	1,008.504
	JB_Points59	13.659	0.817	547.807	2.695	975.073	95.655	0.698	4,089.496	2.992	4.6	1,008.309
	JB_Points60	12.599	0.819	521.256	2.780	975.269	92.372	0.689	3,779.379	2.870	4.3	1,008.309
	JB_Points63	12.713	0.987	574.117	2.878	975.269	90.996	0.553	3,440.688	2.782	4.0	1,008.700
	JB_Points64	13.088	0.631	487.739	2.666	975.660	92.683	0.651	3,721.196	2.854	4.2	1,008.895
	JB_Points65	13.491	0.745	566.837	2.895	975.073	94.514	0.680	4,270.497	3.185	5.1	1,008.309
	JB_Points66	13.320	0.725	491.280	2.554	975.660	92.385	0.656	3,723.374	2.859	4.3	1,009.091
	JB_Points68	12.760	0.620	438.320	2.465	975.660	93.861	0.561	3,274.705	2.556	3.4	1,008.895
JB39	JB_Points69	40.289	0.982	2071.293	3.291	974.291	68.331	0.901	3,608.680	3.467	5.8	1,007.136
	JB_Points72	69.601	0.958	3,654.670	3.389	974.096	68.852	0.966	3,820.453	3.571	6.0	1,006.940
	JB_Points78	12.763	0.986	758.537	3.813	973.314	82.491	0.967	4,764.442	3.719	6.4	1,005.767
	JB_Points80	12.970	0.956	674.335	3.357	973.900	86.656	0.899	4,557.209	3.453	5.8	1,006.745
	JB_Points84	51.412	0.971	3,678.692	4.640	972.532	54.838	0.986	3,892.660	4.570	8.3	1,005.181
	JB_Points85	58.107	0.966	3,584.590	3.988	973.118	57.305	0.977	3,788.342	4.259	7.6	1,005.572
	JB_Points86	53.225	0.986	3,197.582	3.856	973.118	51.276	0.974	3,400.902	4.277	7.7	1,005.767
	JB_Points87	12.765	0.822	686.892	3.632	972.923	91.042	0.907	5,260.163	3.792	6.6	1,005.572
	JB_Points88	11.937	0.858	776.612	4.360	972.336	87.021	0.940	5,882.446	4.409	7.9	1,005.181
	JB_Points89	11.818	0.777	693.871	4.030	972.727	90.310	0.906	5,953.288	4.343	7.8	1,005.181
	JB_Points91	10.716	0.987	805.760	4.861	972.141	71.087	0.988	5,414.262	4.911	9.0	1,004.399
	JB_Points92	13.393	0.988	789.764	3.780	973.705	87.881	0.843	5,001.379	3.812	6.6	1,006.158

Abbreviation: FWHM, full width at half-maximum. HWHM, half width at half maximum.

FIGURE 7 Kernel density plot of the measured zircon (U–Th)/He ages and the best fitted model between the measured ages and calculated ages. Grey curve: kernel density plot of the 20 measured zircon crystals (calculated by DensityPlotter, Vermeesch, 2012); cycles: single zircon crystals; inset shows cumulative plot of ZHe ages; horizontal line in the insert: the real measured single detrital zircon crystals' He-ages; curve in the insert: the best fit line between the real data and the calculated model; K–S test: the Kolmogorov–Smirnov test (method after Press, Flannery, Teukolsky, & Vetterling, 1996); RMS: the goodness of fit between the calculated model and the measured data, the lower the value the better (method after Cserepes, 1989); bins in the insert: the error of the model
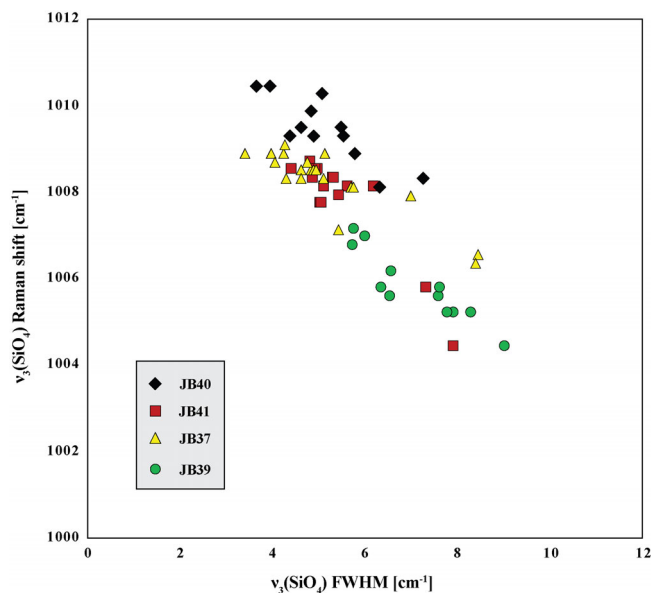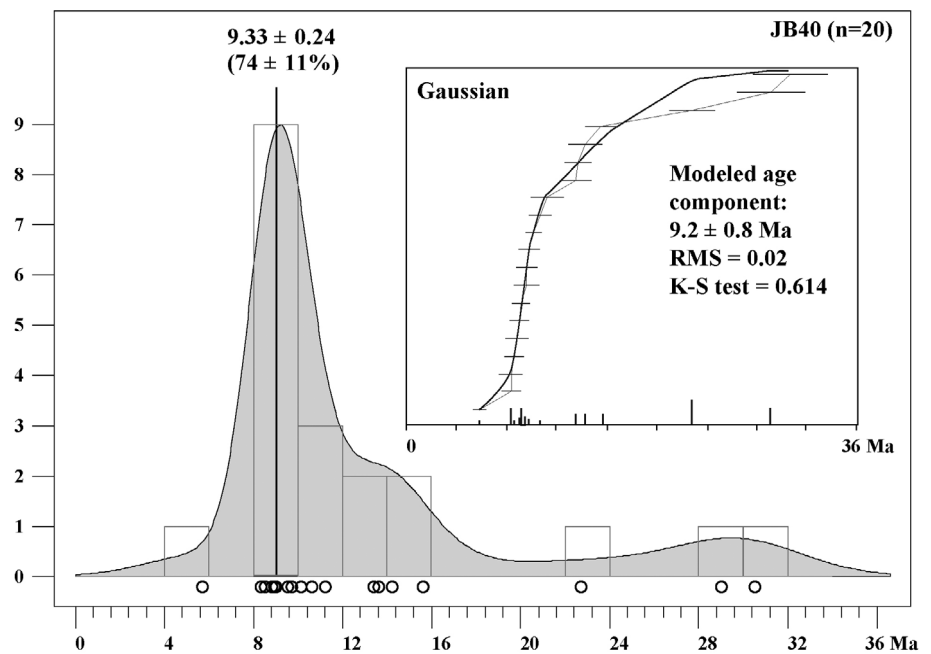
FIGURE 8 Plot of Raman shift versus the full width at half-maximum of the $\nu_3(SiO_4)$ vibration (FWHM) for the sand sample JB40 and the three granitoid samples [Colour figure can be viewed at wileyonlinelibrary.com]

sand. For the proper evaluation of the potential thermal overprint, we should first review the cooling age pattern of the basement that experienced no thermal overprint by young basalt eruptions. Zircon U–Pb studies indicate that the emplacement ages of the granitoid rocks in Huanan and its adjacent areas are Pre-Mesozoic, mostly Early to Middle Permian (Bi et al., 2014; Dong et al., 2017; Yang, Ge, Zhao, Yu, & Zhang, 2015) (Figure 2). Low-temperature thermochronology performed on basement samples far from basalt occurrences yield Early Cretaceous to early Late Cretaceous ZHe ages (136–94 Ma; Figures 2

and 4; Table 1). These ages are considerably older than the ZHe age of sand sample from below the basalt lava. The zircons in the loose sand layer overlying the granitoid basement thus do not carry the regional cooling age signature, instead, their ZHe ages are mostly determined by the thermal effect of the basalt lava.

Zircon He diffusion experiments on pristine crystals reveal that the closure temperature of the ZHe thermochronometer is around 160–200°C in case of duration of the thermal overprint in the range of millions of years (Reiners et al., 2004). Even though the eruption temperature of the overlying basalt lava could be variable, the temperature of basaltic lavas is mostly above 950°C (Francis, 1993). Blondes et al. (2007) presented calculations on the necessary time and temperature relations for reset of the ZHe thermochronometer in case of very short, shock-like thermal events like contact with lava. The laboratory derived He-in-zircon diffusion experiments indicated that partly or complete He loss in xenolithic zircon crystals should happen in magmatic entrainment or contact time of less than 1 hr (Blondes et al., 2007). The sample JB40 experienced proper temperature–time integral for complete reset as it situated close enough to the basalt lava and the heat of the basalt lava could lead to the full removal of the pre-eruption accumulated radiogenic helium from the majority of the zircon grains.

The Raman spectra of well-ordered zircon crystals show distinct, narrow vibrational modes in the spectral range from 200 to 1,010 cm^{-1}. With increasing radiation damage, all of the main Raman bands of the zircon crystals decrease in intensity and become increasingly broader (Nasdala et al., 2001). The FWHM [the full width at half-maximum of the $\nu_3(SiO_4)$ vibration] of the $\nu_3(SiO_4)$ Raman band varies from <3 cm^{-1} in very well ordered ZrSiO$_4$ to more than 30 cm^{-1} in zircons of high amount of accumulated radiation damage. The position and the width of the ~1,000 cm^{-1} peak typically show a well-developed correlation. However, for heat-treated zircons Geisler,
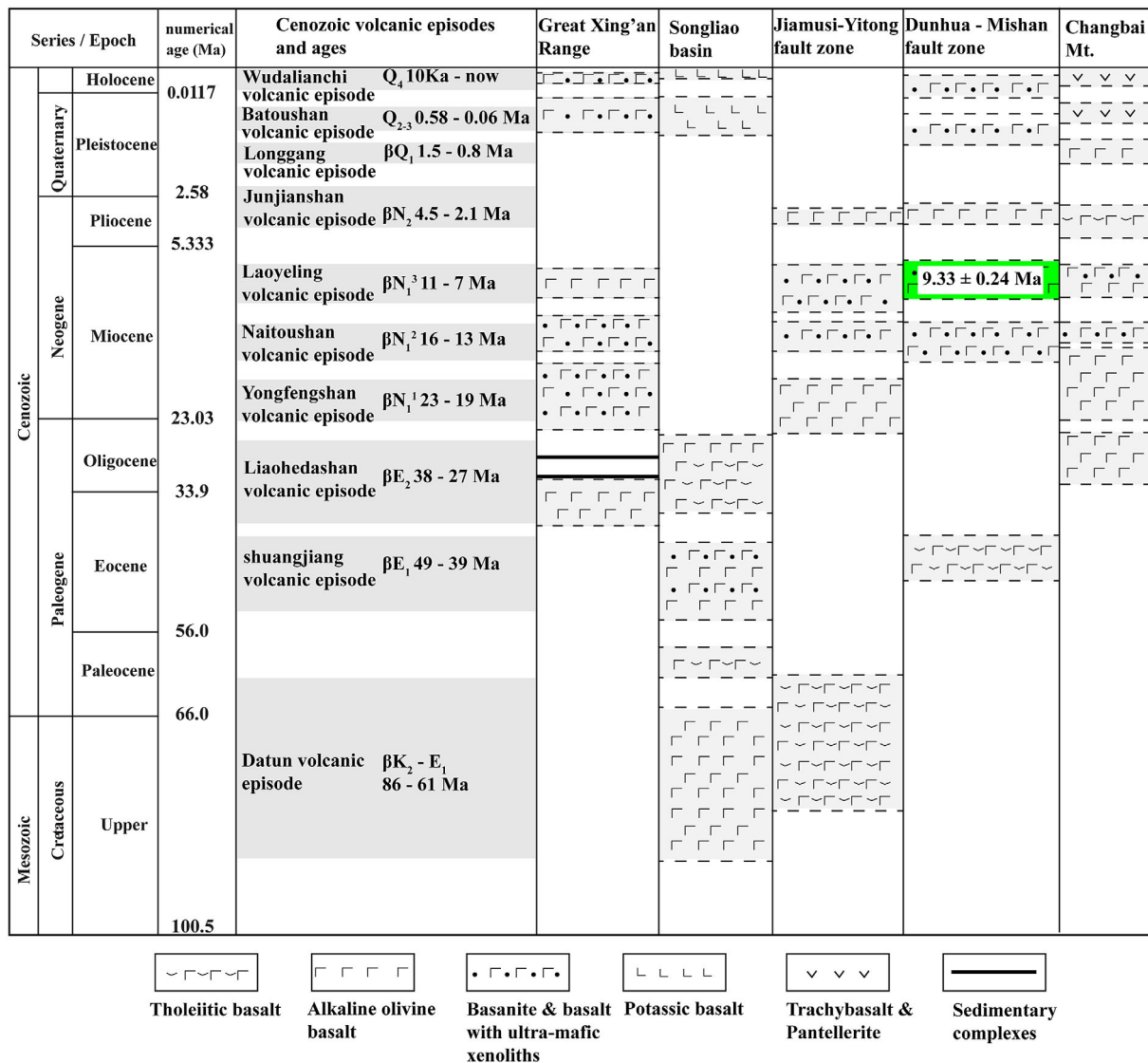
FIGURE 9 Age and major rock types of the 10 Cenozoic volcanic formations in Northeast China (modified after Liu, 1988). Green bar indicates the age of the basalt eruption dated by the JB40 sample of this study [Colour figure can be viewed at wileyonlinelibrary.com]

Ulonska, Schleicher, Pidgeon, and van Bronswijk (2001) and Nasdala, Irmer, and Jonckheere (2002) have found some miscorrelation between the Raman bandwidths and positions. These annealed zircon crystals mostly plot above the peak position-peak width trend established for zircons derived from unheated or slowly cooled geological settings (Nasdala et al., 2001, 2002). In our case, the Raman parameters obtained on sample JB40 plot somewhat off the trend constrained by the three granite samples reflecting the regional cooling history (Figure 8). This property of the lattice of the zircons from the sand sample below the lava flow supports their shock-like thermal reset.

In summary, we can conclude that the detrital zircon crystals have been heated and their ZHe clock became fully reset at the contact with the basalt. The ZHe age of 9.33 ± 0.24 Ma of the sand sample is

thus interpreted to represent the eruption age of the overlying basalt lava.

5.3 | Relation to other Miocene basalt lava occurrences

Liu distinguished 10 Cenozoic volcanic episodes in NE China, which are listed in Figure 9. According to the measured age, the Huanan basalt lava in this study belongs to the Laoyeling volcanic episode (βN_1^3, 11–7 Ma), which is characterized by alkali olivine basalt, basanite, and basalt with ultramafic xenoliths. The magma of this volcanic episode mainly originated from partial melting of the upper mantle caused by extension of the East Asian continent, driven by the slab

rollback of the Pacific plate's westward subduction (Xu et al., 2012; Xu & Fan, 2015).

6 | CONCLUSIONS

1 (U–Th)/He dating of detrital zircon grains from a sand layer directly below a basalt lava flow in the Huanan region reveals a dominant age component of 9.33 ± 0.24 Ma. This implies, together with the Raman data that the reset of the ZHe thermochronometer was caused by the thermal effect of the basalt lava, which erupted at this time.

2 The result also implies that the basalt in the Huanan area belongs to the Laoyeling volcanic episode.

3 As a well-developed weathering insensitive geochronometer, the zircon (U–Th)/He method provides a fast and high accuracy dating tool for young, mafic volcanic rocks.

ORCID

Jianping Zhou https://orcid.org/0000-0002-2573-4364
Yongjiang Liu https://orcid.org/0000-0002-9409-3425
Weimin Li https://orcid.org/0000-0003-0206-2064

REFERENCES

Bai, Z. D., Tian, M. Z., Wu, F. D., Xu, D. B., & Li, T. J. (2005). Yanshan, Gaoshan-two active volcanoes of the volcanic cluster in Arshan, Inner Mongolia. *Earthquake Research in China*, 19(4), 402–408 (in Chinese with English abstract).

Bai, Z. D., Wang, J. M., Xu, G. L., Liu, L., & Xu, D. B. (2008). Quaternary Volcano Cluster of Wulanhada, Right-back-banner, Chabaer, Inner Mongolia. *Acta Petrologica Sinica*, 24(11), 2585–2594 (in Chinese with English abstract).

Basu, A. R., Wang, J. W., Huang, W. K., Xie, G. H., & Mitsunobu, T. (1991). Major element, REE, and Pb, Nd and Sr isotopic geochemistry of Cenozoic volcanic rocks of eastern China: Implications for their origin from suboceanic-type mantle reservoirs. *Earth and Planetary Science Letters*, 105(1–3), 149–169.

Bi, J. H., Ge, W. C., Yang, H., Zhao, G. C., Yu, J. J., Zhang, Y. L., & Tian, D. X. (2014). Petrogenesis and tectonic implications of Early Paleozoic granitic magmatism in the Jiamusi Massif, NE China: Geochronological, geochemical and Hf isotopic evidence. *Journal of Asian Earth Sciences*, 96, 308–331.

Blackburn, T. J., Stockli, D. F., & Walker, J. D. (2007). Magnetite (U–Th)/He dating and its application to the geochronology of intermediate to mafic volcanic rocks. *Earth and Planetary Science Letters*, 259(3–4), 360–371.

Blondes, M. S., Reiners, P. W., Edwards, B. R., & Biscontini, A. (2007). Dating young basalt eruptions by (U–Th)/He on xenolithic zircons. *Geology*, 35(1), 17–20.

Cook, K. L., Royden, L. H., Burchfiel, B. C., Lee, Y. H., & Tan, X. (2013). Constraints on Cenozoic tectonics in the southwestern Longmen Shan from low-temperature thermochronology. *Lithosphere*, 5(4), 393–406.

Cooper, F. J., van Soest, M. C., & Hodges, K. V. (2011). Detrital zircon and apatite (U–Th)/He geochronology of intercalated baked sediments: A new approach to dating young basalt flows. *Geochemistry, Geophysics, Geosystems*, 12(7), 1–8.

Cserepes, L. (1989). *Numerical mathematics—For geophysicist students* (p. 358). Budapest. Tankönyvkiadó.

Dawson, P., Hargreave, M. M., & Wilkinson, G. R. (1971). The vibrational spectrum of zircon ($ZrSiO_4$). *Journal of Physics C: Solid State Physics*, 4(2), 240.

Devroye, L. (1987). *A course in density estimation*. Cambridge, MA: Birkhauser Boston.

Dong, Y., Ge, W. C., Yang, H., Xu, W. L., Bi, J. H., & Wang, Z. H. (2017). Geochemistry and geochronology of the Late Permian mafic intrusions along the boundary area of Jiamusi and Songnen-Zhangguangcai Range massifs and adjacent regions, northeastern China: Petrogenesis and implications for the tectonic evolution of the Mudanjiang Ocean. *Tectonophysics*, 694, 356–367.

Dunkl, I., & Székely, B. (2002). Component analysis with visualization of fitting—PopShare, a Windows program for data analysis. Goldschmidt Conference Abstracts 2002. *Geochimica et Cosmochimica Acta*, 66 (15A), 201.

Fan, Q., & Hooper, P. R. (1991). The Cenozoic basaltic rocks of eastern China: Petrology and chemical composition. *Journal of Petrology*, 32(4), 765–810.

Fan, Q. C., Liu, R. X., & Sui, J. L. (1999). Petrology and geochemistry of rift type Wudalianchi K-rich volcanic rock zone. *Geological review*, 45 (Suppl.), 358–368 (in Chinese with English abstract).

Fan, Q. C., Liu, R. X., Zhang, G. H., & Sui, J. (1998). The genesis and evolution of bimodal volcanic rocks in Wangtian'e volcano, Changbaishan. *Acta Petrologica Sinica*, 14(3), 305–317 (in Chinese with English abstract).

Fan, Q. C., Sui, J. L., Wang, T. H., Li, N., & Sun, Q. (2007). History of volcanic activity, magma evolution and eruptive mechanisms of the Changbai volcanic province. *Geological Journal of China Universities*, 13 (2), 175–190 (in Chinese with English abstract).

Fan, Q. C., Sun, Q., Li, N., & Wang, T. H. (2006). Holocene volcanic rocks in Jingbo Lake Region – Diversity of magmatism. *Progress in Natural Science*, 16(1), 65–71 (in Chinese with English abstract).

Fan, Q. C., Zhao, Y. W., Li, D. M., Wu, Y., Sui, J. L., & Zheng, D. W. (2011). Studies on Quaternary volcanism stages of Halaha River and Chaoer River area in the Great Xing'an Range: Evidence from K-Ar dating and volcanic geology features. *Acta Petrologica Sinica*, 27(10), 2827–2832 (in Chinese with English abstract).

Fan, Q. C., Zhao, Y. W., Sui, J. L., Li, D. M., & Wu, Y. (2012). Studies on Quaternary volcanism stages of Nuomin river area in the Great Xing'an Range: Evidence from petrology, K-Ar dating and volcanic geology features. *Acta Petrologica Sinica*, 28(4), 1092–1098 (in Chinese with English abstract).

Fanale, F. P., & Kulp, J. L. (1962). The helium method and the age of the Cornwall, Pennsylvania magnetite ore. *Economic Geology*, 57(5), 735–746.

Farley, K. A. (2002). (U-Th)/He dating: Techniques, calibrations, and applications. *Reviews in Mineralogy and Geochemistry*, 47(1), 819–844.

Farley, K. A., Wolf, R. A., & Silver, L. T. (1996). The effects of long alpha-stopping distances on (U-Th)/He ages. *Geochimica et Cosmochimica Acta*, 60(21), 4223–4229.

Flower, M., Tamaki, K., & Hoang, N. (1998). Mantle extrusion: A model for dispersed volcanism and DUPAL-like asthenosphere in East Asia and the western Pacific. *Mantle Dynamics and Plate Interactions in East Asia*, 27, 67–88.

Flowers, R. M., Ketcham, R. A., Shuster, D. L., & Farley, K. A. (2009). Apatite (U–Th)/He thermochronometry using a radiation damage accumulation and annealing model. *Geochimica et Cosmochimica Acta*, *73*(8), 2347–2365.

Francis, P. (1993). *Volcanoes: A planetary perspective* (p. 443). Oxford: Clarendon Press.

Galbraith, R. F. (1998). The trouble with "probability density" plots of fission track ages. *Radiation Measurements*, *29*(2), 125–131. http://dx.doi.org/10.1016/s1350-4487(97)00247-3.

Galbraith, R. F. (2010). On plotting OSL equivalent doses. *Ancient TL*, *28*(1), 1–10.

Geisler, T., Ulonska, M., Schleicher, H., Pidgeon, R. T., & van Bronswijk, W. (2001). Leaching and differential recrystallization of metamict zircon under experimental hydrothermal conditions. *Contributions to Mineralogy and Petrology*, *141*(1), 53–65.

Gordon Gastil, R., DeLisle, M., & Morgan, J. (1967). Some effects of progressive metamorphism on zircons. *Geological Society of America Bulletin*, *78*, 879–906.

Guenthner, W. R., Reiners, P. W., Ketcham, R. A., Nasdala, L., & Giester, G. (2013). Helium diffusion in natural zircon: Radiation damage, anisotropy, and the interpretation of zircon (U-Th)/He thermochronology. *American Journal of Science*, *313*(3), 145–198.

HBGMR (Heilongjiang Bureau of Geology and Mineral Resources). (1993). *Regional Geology of Heilongjiang Province* (pp. 347–418). Beijing, China: Geological Publishing House (in Chinese).

Hernandez Goldstein, E., Stockli, D., Ketcham, R., & Seman, S. (2014). (U-Th)/He dating of magnetites in serpentinites. Goldschmidt conference abstracts

Hu, S. L., Wang, S. S., Liu, J. Q., Sang, H. Q., Qiu, J., & Jiang, W. Y. (1983). K-Ar ages and some characters of strontium, oxygen isotopes in Cenozoic Wudalianchi Basalts, Northeast China. *Petrology Research*, *2*, 22–31 (in Chinese with English abstract).

Hurford, A. J., Fitch, F. J., & Clarke, A. (1984). Resolution of the age structure of the detrital zircon populations of two Lower Cretaceous sandstones from the Weald of England by fission track dating. *Geological Magazine*, *121*, 269–277.

Irmer, G. (1985). On the influence of the apparatus function on the determination of scattering cross sections and lifetimes from optical phonon spectra. *Experimentelle Technik der Physik*, *33*, 501–506.

Jahn, B. M., Wu F. Y., & Chen B. (2000). Granitoids of the Central Asian Orogenic Belt and continental growth in the Phanerozoic. *Earth and Environmental Science Transactions of the Royal Society of Edinburgh*, *91* (1-2), 181–193. http://dx.doi.org/10.1017/s0263593300007367.

Liu, J. Q. (1987). Study on geochronology of the Cenozoic volcanic rocks in Northeast China. *Acta Petrologica Sinica*, *4*(2), 21–31 (in Chinese with English abstract).

Liu, J. Q (1988). The Cenozoic volcanic episodes in northeast China. *Acta Petrologica Sinica*, *1*(1), 2–10 (in Chinese with English abstract).

Liu, R. X. (1992). The K-Ar age and tectonic environment of Cenozoic volcanic rock in China. *The Age and Geochemistry of Cenozoic Volcanic Rock in China*, (1–43). Beijing: Seismological Press.

Liu, J. Q., Chen, L. H., Zhong, Y., Lin, W. H., & Wang, X. J. (2017). Petrological, K-Ar chronological and volcanic geological characteristics of Quaternary Xunke high-Mg# andesites from the Lesser Khingan Range. *Acta Petrologica Sinica*, *33*(1), 31–40 (in Chinese with English abstract).

Liu, R., Fan, Q., Zheng, X., Zhang, M., & Li, N. (1998). The magma evolution of Tianchi volcano, Changbaishan. *Science in China Series D: Earth Sciences*, *41*(4), 382–389 (in Chinese with English abstract).

Liu, Y., Li, W., Feng, Z., Wen, Q., Neubauer, F., & Liang, C. (2017). A review of the Paleozoic tectonics in the eastern part of Central Asian Orogenic Belt. *Gondwana Research*, *43*, 123–148.

Liu, Y. J., Zhang, X. Z., Jin, W., Chi, X. G., Wang, C. W., Ma, Z. H., & Zhao, X. F. (2010). Late Paleozoic tectonic evolution in northeast China. *Geology in China*, *37*(4), 943–951 (in Chinese with English abstract).

Lünsdorf, N. K., & Lünsdorf, J. O. (2016). Evaluating Raman spectra of carbonaceous matter by automated, iterative curve-fitting. *International Journal of Coal Geology*, *160*, 51–62.

McDougall, I., & Harrison, T. M. (1999). *Geochronology and thermochronology by the $^{40}Ar/^{39}Ar$ method*. New York, NY: Oxford University Press.

Nasdala, L., Irmer, G., & Jonckheere, R. (2002). Radiation damage ages: Practical concept or impractical vision? Reply to two comments on "Metamictisation of natural zircon: Accumulation versus thermal annealing of radioactivity-induced damage", and further discussion. *Contributions to Mineralogy and Petrology*, *143*(6), 758–766.

Nasdala, L., Irmer, G., & Wolf, D. (1995). The degree of metamictization in zircons: A Raman spectroscopic study. *European Journal of Mineralogy-Ohne Beihefte*, *7*(3), 471–478.

Nasdala, L., Wenzel, M., Vavra, G., Irmer, G., Wenzel, T., & Kober, B. (2001). Metamictisation of natural zircon: Accumulation versus thermal annealing of radioactivity-induced damage. *Contributions to Mineralogy and Petrology*, *141*(2), 125–144.

Press, W. H., Flannery, B. P., Teukolsky, S. A., & Vetterling, W. T. (1996). *Numerical recepies in Pascal* (p. 760). Cambridge, England: Cambridge University Press.

Qiu, J. X., Liao, Q. A., & Liu, M. H. (1991). *Potassium–rich volcanic rocks in Wudalianchi–Keluo–Erkeshan* (pp. 85–95). Wuhan, China: China University of Geosciences Press (in Chinese).

Qiu, Z. L., Yang, J. H., Yang, S. F., Yang, S., Li, C., Wang, Y., ... Yang, X. (2007). Trace element and Hafnium isotopes of Cenozoic basalt-related zircon megacrysts at Muffling, Heilongjiang Province, Northeast China. *Acta Petrologica Sinica*, *23*(2), 481–492 (in Chinese with English abstract).

Reiners, P. W. (2005). Zircon (U-Th)/He thermochronometry. *Reviews in Mineralogy and Geochemistry*, *58*(1), 151–179.

Reiners, P. W., Spell, T. L., Nicolescu, S., & Zanetti, K. A. (2004). Zircon (U-Th)/He thermochronometry: He diffusion and comparisons with 40Ar/39Ar dating. *Geochimica et Cosmochimica Acta*, *68*(8), 1857–1887.

Ren, J., Niu, B., Wang, J., Jin, X., Zhao, L., & Liu, R. (2013). Advances in research of Asian geology—A summary of 1: 5M International Geological Map of Asia project. *Journal of Asian Earth Sciences*, *72*, 3–11.

Renne, P. R. (2000). K-Ar and 40Ar/39Ar dating. *Quaternary Geochronology: Methods and Applications*, *4*, 77–100.

Şengör, A. M. C., Natal'ln, B. A., & Burtman, V. S. (1993). Evolution of the Altaid tectonic collage and Palaeozoic crustal growth in Eurasia. *Nature*, *364*(6435), 299–307.

Shuster, D. L., Flowers, R. M., & Farley, K. A. (2006). Radiation damage and helium diffusion kinetics in apatite. *Geochimica et Cosmochimica Acta*, *70*(18), A590.

Silverman, B. (1986). *Density estimation for statistics and data analysis*. London, England: Chapman and Hall.

Vermeesch, P. (2012). On the visualisation of detrital age distributions. *Chemical Geology*, *312-313*, 190–194.

von Eynatten, H., & Dunkl, I. (2012). Assessing the sediment factory: The role of single grain analysis. *Earth-Science Reviews*, *115*(1–2), 97–120.

Wang, S. S., Liu, J. Q., Zhu, M., & Zhao, D. Z. (1983). K-Ar dating of Cenozoic volcanic-rocks in Changbai Mountains area. *Scientia Geologica Sinica*, (3), 205–216 (in Chinese with English abstract).

Windley, B. F., Alexeiev D., Xiao W. J., Kröner A., & Badarch G. (2007). Tectonic models for accretion of the Central Asian Orogenic Belt. *Journal of the Geological Society*, *164*(1), 31–47. http://dx.doi.org/10.1144/0016-76492006-022.

Xu, Y. G., & Fan, Q. C. (2015). Cenozoic valcanism in Eastern China: Review and perspectives. *Bulletin of Mineralogy, Petrology and Geochemistry*, *34*(4), 682–689 (in Chinese with English abstract).

Xu, Y. G., Zhang, H. H., Qiu, H. N., Ge, W. C., & Wu, F. Y. (2012). Oceanic crust components in continental basalts from Shuangliao, Northeast China: Derived from the mantle transition zone? *Chemical Geology*, *328*, 168–184.

Yang, H., Ge, W., Zhao, G., Yu, J., & Zhang, Y. (2015). Early Permian–Late Triassic granitic magmatism in the Jiamusi–Khanka Massif, eastern segment of the Central Asian Orogenic Belt and its implications. *Gondwana Research*, *27*(4), 1509–1533.

Yin, J. H., Jull, A. T., Burr, G. S., & Zheng, Y. G. (2012). A wiggle-match age for the Millennium eruption of Tianchi Volcano at Changbaishan, Northeastern China. *Quaternary Science Reviews*, *47*, 150–159. http://dx.doi.org/10.1016/j.quascirev.2012.05.015.

Zhang, H. H., Xu, Y. G., Ge, W. C., & Ma, J. L. (2006). Geochemistry of Late Mesozoic-Cenozoic basalts in Yitong-Datun area, Jilin Province and its implication. *Acta Petrologica Sinica*, *22*(6), 1579–1596 (in Chinese with English abstract).

Zhang, Z. C., Li, Z. N., Li, S. C., Xin, Y., Li, Z. M., & Wang, X. Z. (2000). Geochemistry of the Jingpohu Holocene basaltic rocks, Hellongjiang Province, and discussion on their deep processes. *Acta Petrologica Sinica*, *16*(3), 327–336 (in Chinese with English abstract).

Zhao, Y. W., Fan, Q. C., Bai, Z. D., Sun, Q., Li, N., Sui, J. L., & Du, X. X. (2008). Preliminary study on Quaternary volcanoes in the Halaha River and Chaoer River area in Daxing'an Mountain Range. *Acta Petrologica Sinica*, *24*(11), 2569–2575 (in Chinese with English abstract).

Zheng, C. Q., Xu, W. L., & Wang, D. Y. (1999). The petrology and mineral chemistry of the deep-seated xenoliths in Mesozoic basalt in Fuxin District from western Liaoning. *Acta Petrologica Sinica*, *25*(4), 616 (in Chinese with English abstract).

Zhou, X. H. (2006). Major transformation of subcontinental lithosphere beneath eastern China in the Cenozoic-Mesozoic: Review and prospect. *Dixue Qianyuan/Earth Science Frontiers*, *13*(2), 50–64 (in Chinese with English abstract).

Zou, H., Fan, Q., & Yao, Y. (2008). U–Th systematics of dispersed young volcanoes in NE China: Asthenosphere upwelling caused by piling up and upward thickening of stagnant Pacific slab. *Chemical Geology*, *255*(1), 134–142.

Zou, H., Zindler, A., Xu, X., & Qi, Q. (2000). Major, trace element, and Nd, Sr and Pb isotope studies of Cenozoic basalts in SE China: Mantle sources, regional variations and tectonic significance. *Chemical Geology*, *171*, 33–47.